We are IntechOpen, the world's leading publisher of Open Access books Built by scientists, for scientists

4,800
Open access books available

122,000
International authors and editors

135M
Downloads

Our authors are among the

154
Countries delivered to

TOP 1%
most cited scientists

12.2%
Contributors from top 500 universities

CLARIVATE ANALYTICS BOOK CITATION INDEX INDEXED

WEB OF SCIENCE™

Selection of our books indexed in the Book Citation Index in Web of Science™ Core Collection (BKCI)

Interested in publishing with us?
Contact book.department@intechopen.com

Numbers displayed above are based on latest data collected.
For more information visit www.intechopen.com

17

Energy Efficient Semiconductor Optical Switch

Liping Sun and Michel Savoie
Communications Research Centre
Canada

1. Introduction

Energy-saving technology that reduces power consumption is of increasing importance due to the ever-increasing demand for Internet services. To prevent the traffic growth from being strangled by energy bottlenecks, novel architectural and technological solutions are indispensable. The most obvious way to cope with the issue is to reduce the energy consumed by the network elements.

Fast optical switching is an important enabler of advanced optical networks, in particular such functions as routing burst and packet optical signals, optical path provisioning and fault restoration. Semiconductor Digital Optical Switches (DOSs) can fulfill such high speed applications due to their nanosecond switching times, step-like switching responses, and immunity to variations in temperature, wavelength, polarization, refractive index and device fabrication tolerances. Moreover, semiconductor DOSs offer the potential for integration with other semiconductor optoelectronic components and thus promise considerable reductions in the size, complexity and cost of an overall optical system.

For optical waveguide switches, fast optical switching may be achieved by a refractive index change, induced either by carrier injection (Zegaoui et al., 2009; Bennett et al., 1990) or by the electro-optic effect (Cao et al., 2009; Agrawal et al., 1995), within III-V semiconductors, such as GaAs-based and InP-based. Compared to carrier-injection switches, electro-optic switches have faster switching speeds but larger switching voltages since the refractive index change induced by an electro-optic effect is about two orders of magnitude smaller than that by carrier injection.

Therefore, until now, most of the commercially available semiconductor DOS products have been based on carrier-injection (Ikezawa et al., 2008). These devices typically utilize carrier-induced Total Internal Reflection (TIR) at a waveguide branching or crossing point to switch the light path from one waveguide to another. Such TIR-based semiconductor switches typically require a large index modulation, e.g. in the order of 0.01, with the region of changed index having a well-defined boundary. Accordingly, efforts have been made to restrict current spreading and to confine the injected carriers to the desired region. Typically, achieving such carrier confinement involves using relatively complex semiconductor device technologies, such as ion implantation (Abdalla et al., 2004; Zhuang et al., 1996), electron-beam lithography (Shimomura et al., 1992), Zn diffusion (Yanagawa et al., 1990), and epitaxial regrowth (Thomson et al., 2008).

A plane view of a typical conventional semiconductor DOS is illustrated in Fig. 1(a), wherein two waveguides intersect at an angle θ forming an X-like waveguide structure. An electrode is provided over a common waveguide region where the waveguides intersect for injecting carriers into a portion of the common region to decrease its refractive index n by an amount Δn sufficient to induce TIR for the input beam and to cause it to turn by the angle θ to form the switched light. In the absence of the carrier injection, i.e. when there is no current flowing through the electrode, the input light continues its propagation along the waveguide past the common region to form the transmitted light. In order to switch the input light, the electrode is positioned so that its edge, which faces the input light, crosses the input waveguide at an angle θ/2. One drawback of the design in Fig. 1 is that, for optimal performance, the electrode should be positioned with its 'receiving' edge centered in the common waveguide region. This makes the structure asymmetrical with respect to the two input waveguides, so that the switch is, essentially, a 'Y' switch that can only function as a 1×2 switch and not as a 2×2 switch.

A typical 2×2 semiconductor TIR DOS with the conventional electrode design is shown in Fig. 1(b). In order to reduce an optical axis misalignment of the reflected light for both input ports, the electrode has to be narrow; disadvantageously, a narrow electrode will generally result in poor reflectivity induced by the current passing through the electrode, leading to a degradation of the switch extinction ratio, i.e. the optical power ratio for the output ports.

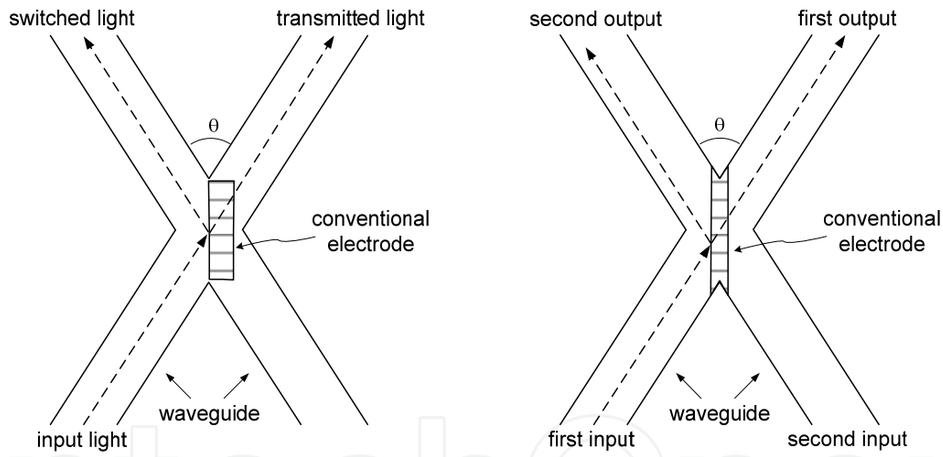

(a) 1×2 (b) 2×2

Fig. 1. Schematic diagrams of TIR optical switches with conventional electrodes.

Fig. 2 is a schematic diagram of a 2×2 switch which has a similar waveguide topology as Fig. 1(b), but utilizes the bow-tie electrode in place of the straight electrode of Fig. 1(b) (Li et al., 2001). The bow-tie electrode has a narrow part located at the central point of the waveguide intersection, and the electrode is symmetrical with respect to all four waveguide ends. The switch has a switching angle θ = 2˚, and an electrode bow-tie angle of 1.5 degrees. The switch utilizes ion implantation about the electrode to decrease current spreading and confine the injected carriers. One disadvantage of the prior art bow-tie electrode design is that its electrode is still narrow at the waveguide crossing point, potentially enabling the light to leak therethrough under the carrier injection condition. Furthermore, a part of the incoming light that incidents on the second electrode segment may be refracted rather than reflected because of the increased grazing angle. All these limit the waveguide crossing

angle θ of the bow-tie type 2×2 switches to about 2° in real device applications. The small switching angle increases the size of the device and limits the integration density.

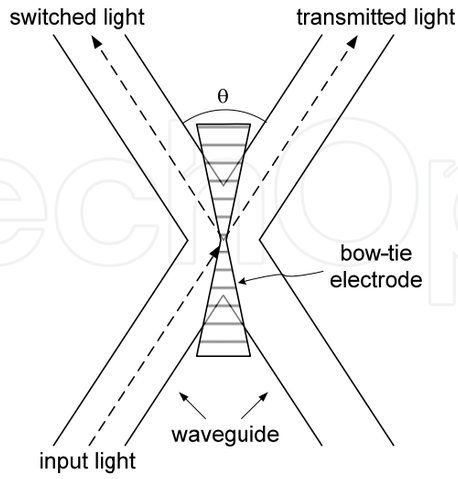

Fig. 2. Schematic diagram of a 2×2 TIR optical switch with bow-tie electrode.

Another disadvantage of the prior art TIR semiconductor switches is their relatively large power consumption, especially for devices with the switching angle at the higher end of the range, as such devices require larger electrical currents. Reconfigurable waveguide DOS devices with small switching current and low crosstalk have been reported recently (Zegaoui et al., 2009; Ng et al., 2007), but their branch angle is only 0.9˚. It is therefore desirable to develop TIR switches with greater deflection angles and reduced power consumption.

This chapter presents our approaches to improve the energy efficiency of semiconductor DOSs for applications in next generation green optical networks. In the following sections, we first propose and demonstrate a novel double-reflection switch design that can reduce the power consumption and increase the switch deflection angle. Then, in the next section, an ultra-low-power 2×2 carrier-injection optical switch based on a Mach-Zehnder Interferometer (MZI) formed by Multi-Mode Interference (MMI) couplers is introduced and investigated. Conclusions and future applications are provided in the last section.

2. Double-reflection TIR DOS

This section discusses the design, fabrication and characterization of a novel double-reflection technique to fabricate 1×2 and 2×2 wide-angle AlGaAs/GaAs carrier-injection TIR optical switches. This new development uses only conventional semiconductor fabrication technologies to reduce the switching current and relax the tight restriction on the width of the electrodes located at the switch centre. To compensate for the increased switching current, compositionally graded interfaces are added at the heterojunctions to reduce the switching voltage and thus the power consumption. Switching performance is further improved by applying curved electrodes and carrier-restriction gaps.

2.1 Double-reflection structure

Our approach to improve the performance and reliability of 1×2 and 2×2 TIR optical switches with a double-reflection electrode geometry is illustrated in the two pictures shown

in Fig. 3 below. The electrode in Fig. 3(a), which utilizes a well known 'Y'-shaped waveguide structure, is shaped to induce double reflection of the input light. Its first edge faces the input waveguide and is positioned for turning, in the presence of the carrier injection, the input light by a first deflection angle θ_1, so as to form the first reflected light that propagates generally towards the second edge. The second edge is positioned for turning the first reflected light by a second angle θ_2 towards the switched output waveguide for coupling thereinto as the switched light. This electrode is also shaped and positioned so that, in the absence of the carrier injection, substantially all or at least most of the input light passes under the first edge of the electrode. This design also results in that in the presence of the carrier injection through the electrode, substantially all or at least most of the input light is reflected at the first edge. Note that this feature differentiates the electrode of Fig. 3(a) from the prior art bow-tie electrode of Fig. 2, wherein the input light impinges upon two inclined edges of the bow-tie in substantially equal portions, so that only about half of the input light passes under each bow-tie edge, resulting in a loss of input light since for a large switch branching angle the part of input light that directly incidents on the second edge of the electrode will not be reflected under TIR due to their increased grazing angle.

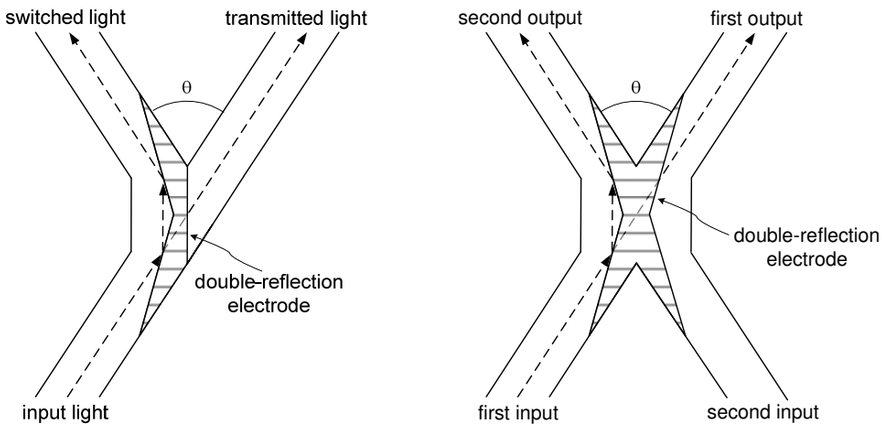

(a) 1×2 (b) 2×2

Fig. 3. Schematic diagrams of TIR optical switches with double-reflection electrode.

Continuing to refer to Fig. 3(a), in a further advantage each of the first and second deflection angles is less than the light switching angle θ, and therefore the switching of the input light's direction by the switching angle θ may be accomplished by a smaller refractive index change Δn under the electrode, and thus using a smaller injection current than would have been required for the conventional single-reflection electrode design such as that of Fig. 1. In one currently preferred electrode geometry design, the first and second angles θ_1, θ_2 are both equal to one half of the branching angle θ, i.e. $\theta_1 = \theta_2 = \theta/2$.

Advantageously, this double-reflection structure enables to have the switching angle θ twice as large as in the conventional single-reflection design for the same refractive index change Δn in the index change region, or, alternatively, to turn the light by the same angle θ using only half of the electrical current. Indeed, the reflective index change Δn that is required to induce the TIR at the first and second edges may be estimated from an approximate TIR condition,

$$\theta_i \leq \Delta n/n, \; i = 1, 2, \tag{1}$$

which approximately holds for $\Delta n/n << 1$ and the angles θ_i measured in radians, so that reducing the turning angle by a factor of 2 reduces the required index change by the same factor.

The double-reflection structure that has been described above for 1×2 optical switches, can be easily adopted for 2×2 switches, such as schematically shown in Fig. 3(b), by adding a second input waveguide and by symmetrically extending the double-reflection electrode so as to provide a second pair of electrode edges for switching the light from the second input waveguide into the first output waveguide by means of double reflection at the third and fourth electrode edges. In the 2×2 switch, the second input waveguide is optically aligned with the second output waveguide so that, in the absence of the carrier injection, input light from the second input waveguide will be transmitted by the branching section into the second output waveguide. In the presence of the carrier injection, light that enters from the second input waveguide experiences two consecutive reflections at the third and fourth edges and is directed into the first output waveguide, while light that enters from the first input waveguide also experiences two consecutive reflections at the first and second edges as described before, and is directed into the second output waveguide. The waveguide and electrode edge structure of the 2×2 switch is substantially symmetrical with respect to an axis of symmetry which bisects the waveguide branching angle. In Fig. 3(b), the electrode is shaped as an 'X', with two cut-outs around the symmetry line in the input and output portions of the structure, so as to reduce the scattering optical loss, the total electrical current required for the switching, and therefore to reduce the power consumption and device heating.

The aforedescribed double-reflection switching addresses important drawbacks of the prior art TIR-based optical switches. It eliminates the optical misalignment problem and electrode width problems of the straight and bow-tie electrodes in the 2×2 switching configurations. As a result, at the same switch crossing angle, the index change, and hence the injection current density, that is required by the TIR condition needs to be only half of that of the prior art "single reflection" design, thereby reducing the injection current density by half for the same switch crossing angle θ. On the other hand, if the same switching current density is to be used as in the prior art TIR-based switches, the switch crossing angle can be doubled, making the overall device more compact and thus allowing more devices to be integrated on a wafer. This newly developed technique enables optical switching at greater waveguide crossing angles θ and/or smaller induced refractive index changes, and thus smaller power consumption.

One potential disadvantage of the aforedescribed multi-reflection switch configuration is that, for the same switch crossing angle θ, the overall area of the switch electrode may be as much as two times larger than that of the prior art single-reflection electrodes, which may partially negate the effect of the reduced current density upon the total power consumption of the device; the larger electrode area and a relatively more complex waveguide branching area may also lead to an increase in the scattering optical loss in the waveguide branching region. Advantageously, these two potentially deleterious effects decrease dramatically by increasing the switch crossing angle θ, and may be reduced to an acceptable level at least for θ greater than about 3-4°.

2.2 Curved electrodes

A schematic layout of our proposed 2×2 switch with double-reflection structure is shown in Fig. 4. Each of the four segments of the switch electrode is curved in a logarithmic spiral

shape instead of the conventional straight electrode. This electrode-curvature has been theoretically studied and reported that it could provide high power reflectivity, high extinction ratio, and low scattering loss (Nayyer et al., 2000).

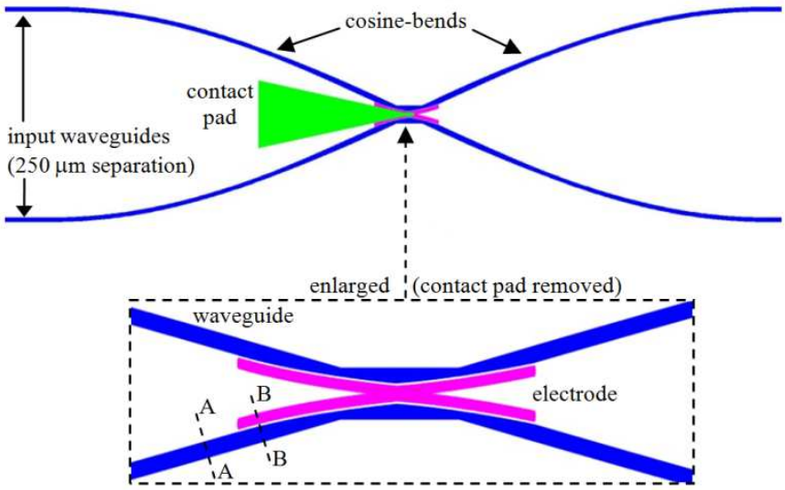

Fig. 4. Schematic layout of a proposed 2×2 double-reflection TIR optical switch.

The fabricated optical switch has the two input waveguides and two output waveguides extended with curved waveguide sections embodied as cosine bends, with a functional form $[h/2-(h/2)\cos(\pi x/l)]$, where h is the height of the bend, l is the length of the bend, and x is the horizontal propagation length. The device further included a top contact pad to provide an electrical contact to the switching electrode for delivering current to the switch electrode. To reduce the crosstalk at the waveguide crossing, adiabatic tapers are used in the waveguide branching region. This waveguide widening can also provide more fabrication freedom for the electrode. As shown in the figure, the double-reflection design enables us to set the electrode width at several times larger than the light penetrating depth and hence provide a sufficient index change for TIR and large extinction ratio.

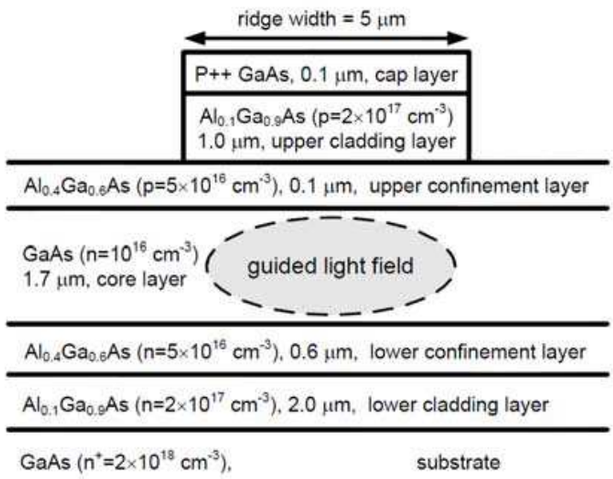

Fig. 5. The waveguide layer structure which specifies the composition ($Al_x Ga_{1-x} As$), doping profile, and layer thickness for each layer.

Fig. 5 is a schematic diagram of the vertical cross-section of the waveguide structure that we used for the 2×2 switch along the line 'A-A' shown in Fig. 4. The switch's strip-loaded waveguide design has a multilayer heterostructure with a W-shaped index profile. The waveguide core layer of GaAs is 1.7 μm thick, and is, to the best of our knowledge, the largest ever reported for a single-mode semiconductor DOS. It provides high coupling efficiency to a single mode fibre.

2.3 Current restriction gap

At the TIR interface inside our switch design, a small isolation gap is introduced between the electrode and waveguide to restrict the current spread into the waveguide regions not covered by the electrode, and to obtain a sharp carrier gradient profile for improved switching efficiency. This current restriction effect of the isolation gap is schematically illustrateed in Fig. 6. It also schematically shows an effective reflection interface wherein the reflection of the guided light occurs in the presence of the carrier injection. When the switching voltage V_b is applied between the switching electrode and a bottom contact, the switching electrical current flows through the current flow region indicated by cross-hatching. Although the gap substantially reduces the current spread into the regions not directly under the switching electrode, it does not eliminate the spreading completely, resulting in the possibility of a small lateral offset of the effective reflection interface from the reflection edge of the electrode. This offset however may be rather small, for example on the order of less than 1 μm, and is smaller than the size of the waveguide branching region.

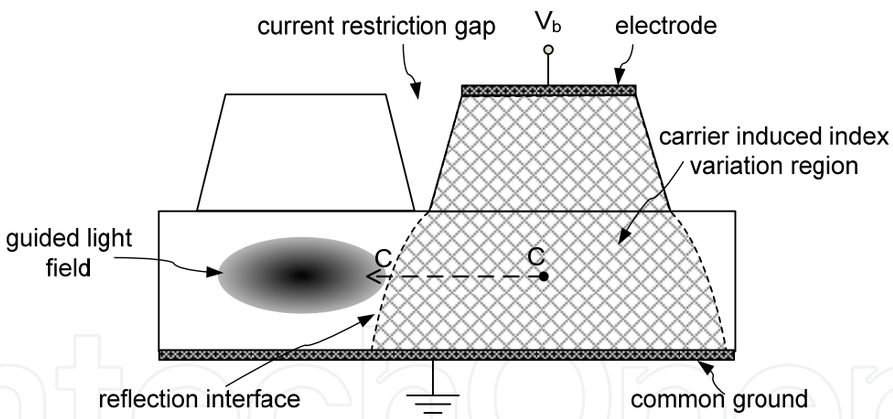

Fig. 6. Schematic diagram of the optical mode, the current flow region and the reflective interface induced by the carrier injection in the cross-sectional view of Fig. 4 taken along the line 'B-B'.

The carrier-induced index variation at the reflection interface is gradual due to the spatial spreading of injection current flow. If an abrupt spatial variation in the carrier concentration or current flow can be formed along the reflection interface, more light can be reflected to the other port. If the waveguide core layer is very thick, it is important to check how the current restriction gap affects the spreading carrier-induced index change profile at the reflection interface.

Fig. 7 is the calculated carrier concentration along line 'C-C', the middle of the core layer, in the cross-section as shown in Fig. 6 with or without a separation gap inside the splitting

region, respectively. Fig. 7 was generated based on a two-dimensional simulation of Δn by using ApSys, a 2D/3D FEM optoelectronic simulation software from Crosslight Software Inc., and is based on a top electrode that is 200 μm long and with a bias current of 200 mA. Only the structure from the centerline of the biased waveguide is shown in Fig. 7. The dotted line in Fig. 7 is the edge of the top electrode. As illustrated in Fig. 7, an isolation gap in the splitting region is needed to prevent carriers from spreading beyond the electrode region. The self-heating effect was also included in the 2D FEM simulation. In the simulation, the room temperature is set at 300 K and the heat generated from contact resistance was not included. Calculation shows that the guiding of light to the destination port via modal evolution is unchanged with or without the self-heating temperature change. Fig. 8 is the corresponding carrier-induced refractive index change Δn along the middle of the core layer with or without a separation gap in the splitting region, respectively. The calculation involves a combination of bandfilling, band-gap shrinkage, and plasma effect (Bennett et al., 1990). The maximum index change is calculated to be -0.037 at the midpoint of the biasing electrode. The TIR interface located under the electrode edge is 2.5 μm apart from the biased waveguide centre. By introducing a current restriction gap inside the switch structure, the index change profile at the reflection interface is much more sharp than a switch without a gap inside. Clearly, more light can be steered into the higher-index waveguide by introducing a small gap in the splitting region.

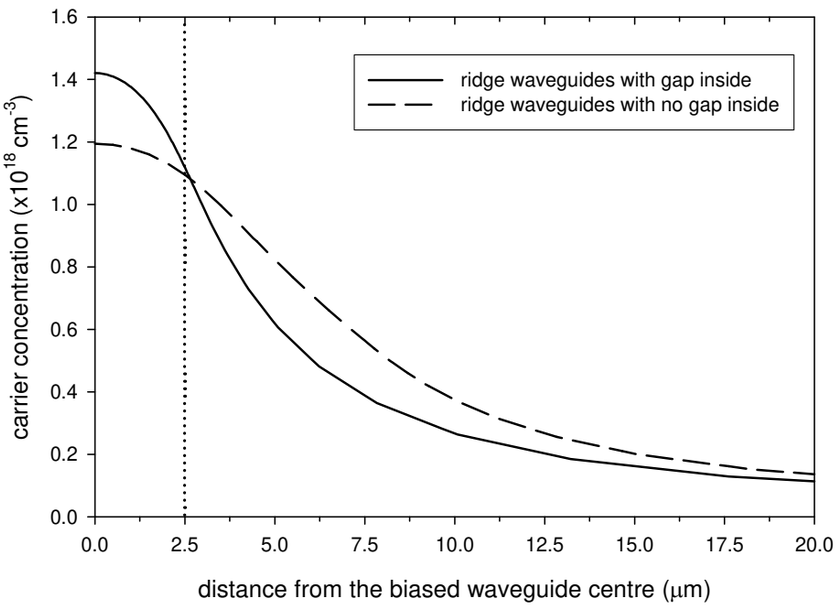

Fig. 7. Carrier concentration along the middle of core layer in the cross section at the junction branching point. The dotted line is the edge of the top electrode.

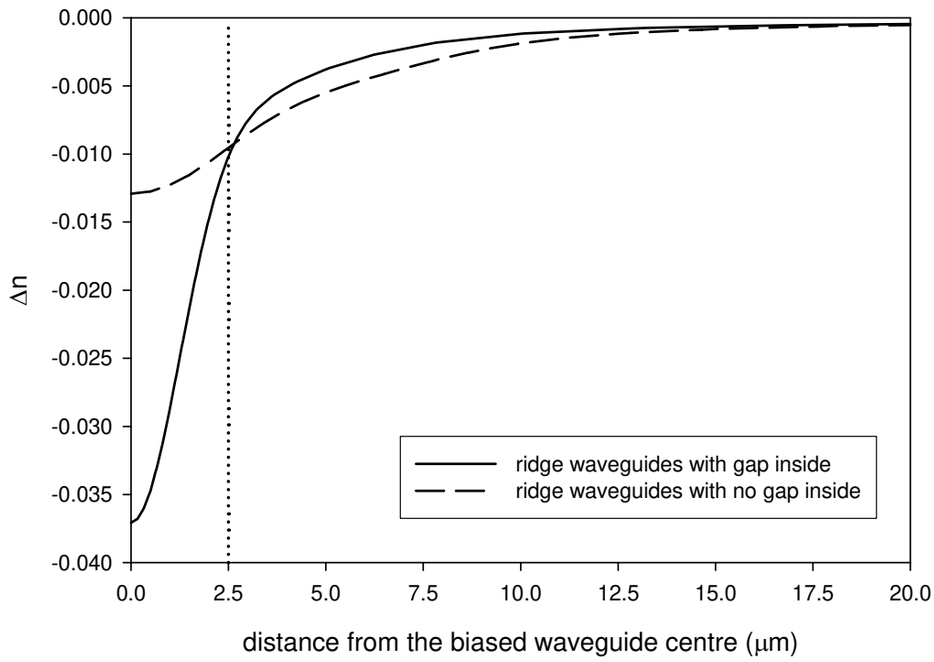

Fig. 8. Carrier-induced refractive index change Δn along the middle of core layer in the cross section at the junction branching point. The dotted line is the edge of the top electrode.

2.4 Graded heterojunction interfaces

The up-to-date growth technology of Metal-Organic Chemical Vapor Deposition (MOCVD) enables us to build semiconductor materials with precise control of thickness and composition at the atomic level. If no grading of the chemical composition of the semiconductor is applied in the vicinity of the heterostructure, all the heterojunction interfaces of the fabricated waveguide using the layer structure shown in Fig. 5 are sharply defined at atomic-level precision. One of the problems introduced by abrupt heterostructure is the band gap discontinuities caused by free charge transferring at the heterojunction between two semiconductors with different bandgap energy (Capasso et al., 1987). Carriers in the large-bandgap material will diffuse over to the small-bandgap material where they occupy band states of lower energy. As a result of the carrier transfer, and electrostatic dipole forms and leads to the band bending. For example, most published results for the $Al_xGa_{1-x}As/GaAs$ heterojunction indicate that the conduction band discontinuity $\Delta E_C \approx 0.24$ eV for x=0.30 (Wang, 1986).

Fig. 9 is the calculated band diagram of the zero-biased waveguide using the abrupt layer and doping structure shown in Fig. 5. The numerical simulation software (the APSYS of Crosslight Software) uses the FEM method to solve a 2D Poisson's equation for potential voltage, continuity equation for carriers, and thermionic emission theory for a bandgap barrier at the heterojunction interface. The adaptive mesh points were set to be very dense near the heterojunction in order to calculate the bandgap barrier correctly. The band spikes shown in Fig. 9 at the double-heterostructure interfaces near the lower confinement layer will suppress the flow of charge carriers across the junction. This band–barrier rectification effect reduces the carrier injection efficiency of the switch. It is therefore desirable to eliminate such spikes in the conduction or valence band.

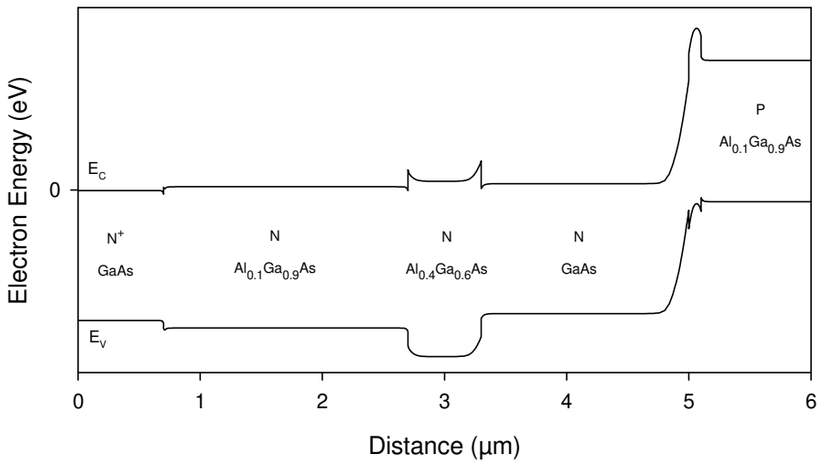

Fig. 9. Band diagram of the zero-biased waveguide using the abrupt layer and doping structure shown in Fig. 5.

Composition grading is a common technique in the design of quantum-well lasers, Hetero-junction Bipolar Transistors (HBTs) and modulation-doped transistors. The compositional grading at the junction interface can smooth out a large part of the band discontinuity so that the carrier injection is increased. Usually a graded barrier with a grading length of a few hundred angstroms can effectively minimize the inference of the band spike at the abrupt interface. The smaller the carrier concentration on either side of the heterojunction, the wider the graded region has to be in order to reduce the spike height. The composition grading effects on band spikes are clearly demonstrated in Fig. 10, which shows the calculated conduction band profiles for the double-heterostructure interfaces at the lower confinement layer. Three cases were studied, varying the length of grading width L. The three simulations are for L=0, L=200 Å and L=400 Å using the layer structure shown in Fig. 5. The metallurgical grading of $Al_xGa_{1-x}As$ was set linear in the grading region.

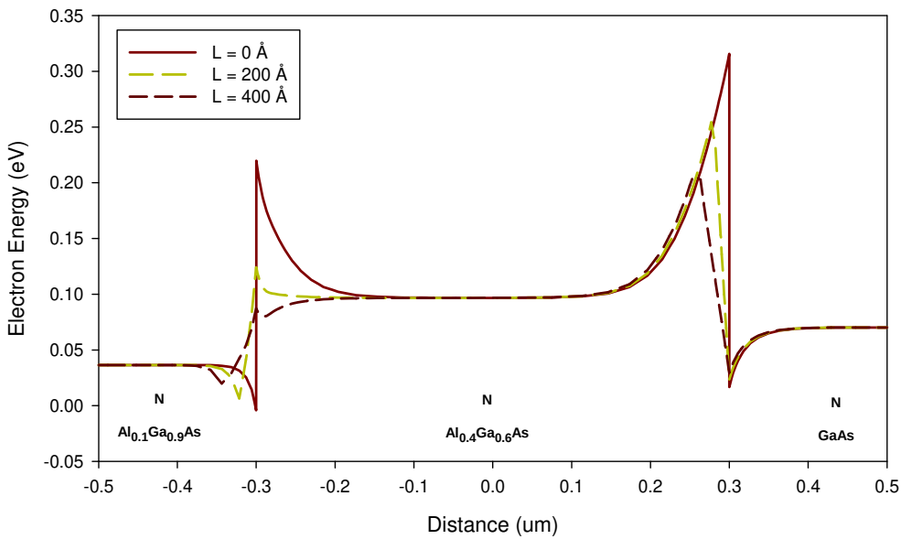

Fig. 10. Conduction band profiles for the double-heterostructure near the lower confinement layer at different grading width L.

The most important advantage of applying graded heterojunctions in the switches is that the reverse bias problem in a multilayer switch structure can be significantly reduced. The n-n heterojunction between $Al_{0.4}Ga_{0.6}As$ and $Al_{0.1}Ga_{0.9}As$ at the bottom of the lower confinement layer (see Fig. 5) would be reverse biased when a voltage is applied to operate the switch. From our simulations, over 80% of the switch driving voltage is applied across the reverse biased n-n heterojunction when all heterojunctions are abrupt. As shown in Fig. 10, this abrupt n-n heterojunction barrier can be effectively reduced or completely eliminated by over 400 Å-length grading. As a result, the switching voltage is further reduced.

2.5 Exemplary demonstrations

A prototype 2×2 carrier-injection optical switch with double-reflection electrode has been developed and fabricated. The waveguide structure, as shown in Fig. 5, has six AlGaAs/GaAs layers grown by MOCVD on an n+ GaAs substrate. For a single-mode waveguide at a wavelength of the input light of 1.55 μm, the ridge width of 5.0 μm was used, with the ridge height of about 1 μm. The GaAs waveguide core layer is lightly doped, $n=10^{16}$ cm^{-3}, to provide an optimized trade-off between low propagation loss and low switching voltage. In order to reduce energy band discontinuities at the heterojunctions that would impede the current flow therethrough, and to reduce the switching voltage, compositionally graded interfaces 20 nm - 40 nm thick were used at all the layer interfaces. The width of the current restriction gap, as illustrated in Fig. 6, is about 1 μm. These gaps may be formed using a double mask technique (van der Tol et al., 1994) to overcome photolithography problems when forming small gaps. With this technique, two masking stripes, which are independently defined in separate lithographic steps, can also be used as masks in a dry etch process to obtain ridge waveguides with small isolation gaps.

Fig. 11 is a Scanning Electron Microscope (SEM) image of the fabricated switch with the input waveguides on the left, viewed from an angle. It should be noted that the fabrication processes only employ conventional technologies, such as UV photolithography, e-beam evaporation and plasma etching. Independently formed electrode and photoresist layers were used as a double-mask in a single dry etch process to form the ridge waveguides and gaps. Uniform gap spacing was obtained using vernier alignment marks with ± 0.1 μm alignment accuracy. Fig. 12 is a SEM picture of the fabricated carrier-restriction gap, with the sample cleaved at a location close to the branching vertex of output waveguides.

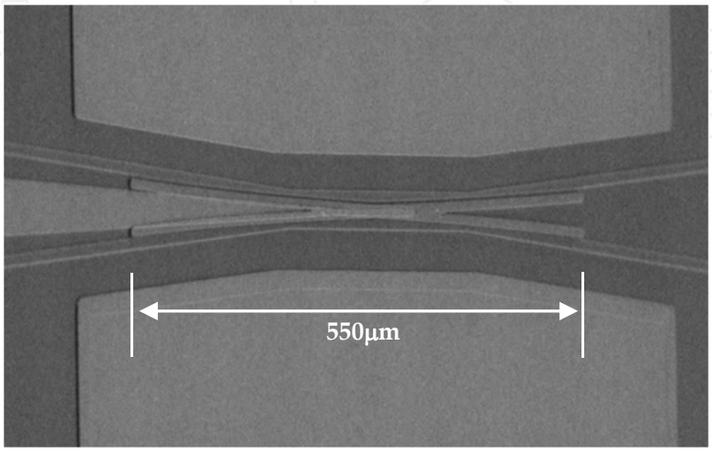

Fig. 11. SEM image of a fabricated 2×2 double-reflection TIR optical switch.

The fabricated switch has an electrode length of 550 μm, a waveguide crossing angle of 7°, and a cosine-bend section of 6.4 mm. The measured propagation losses of straight waveguides with undoped and lightly doped core layers are 0.3 dB/cm and 1.5 dB/cm, respectively, for a wavelength of 1.55 μm. Fig. 13 is the measured switching curves for light coupled into the top left input port. The switched state was obtained for an injection current of 220 mA. At this state, the driving voltage was 2.89 V and the measured device series resistance was 9.8 Ω. So the total power dissipation was at a manageable level of 0.6 W. With the area of the fabricated electrode being 3400 μm^2, the corresponding switching current density was 6.5 kA/cm^2. By using this current density and assuming a 10 ns carrier lifetime, the estimated carrier density and Δn are about 2×10^{18} cm^{-3} and -0.02, respectively. Such a high index change may be the result of two facts: one is that the carrier lifetime is quite long in the thick core layer; the other is that the current spreading decreases at very high current densities which results in current "bunching" in the core below the isolation gap and hence yields better power reflectivity. The measured switching time is 15 ns. On-off extinction ratio is 13 dB for the through port and 14 dB for the switched port. The switch is wavelength independent for a wavelength range from 1540 nm to 1570 nm. A very small polarization dependence of TE and TM modes has been observed (<0.5 dB). The measured extra insertion loss of the 2×2 switch compared with the straight waveguide fabricated on the same chip is 3 dB.

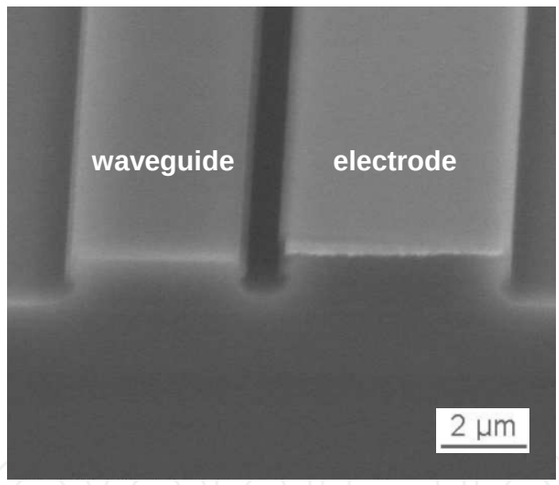

Fig. 12. SEM image of the carrier-restriction gap in an angled view of Fig. 4 taken along the line B-B.

Similarly, we also developed a 1×2 double-reflection optical switch which has a measured total power dissipation of 0.24 W with no extra cooling required to keep the switched state. As shown in Fig. 14, the fabricated switch has an electrode length of 480 μm, and a waveguide crossing angle of 6°. Based on the measured switching curve shown in Fig. 15, the switched state was obtained for an injection current of 105 mA at a bias of 2.30 V. The on-off extinction ratio is 15 dB for the through port and 14 dB for the switched port. The measured extra insertion loss of the 1×2 switch is 2 dB compared with the straight waveguide fabricated on the same chip. The switch is wavelength independent for the measured C-band. The polarization dependence of TE and TM modes input lights has been found to be less than 0.5 dB. The measured switching time is 11 ns which is close to the

carrier lifetime in bulk materials. Reducing the guiding layer thickness would increase the switching speed but at the cost of decreasing the fibre coupling efficiency.

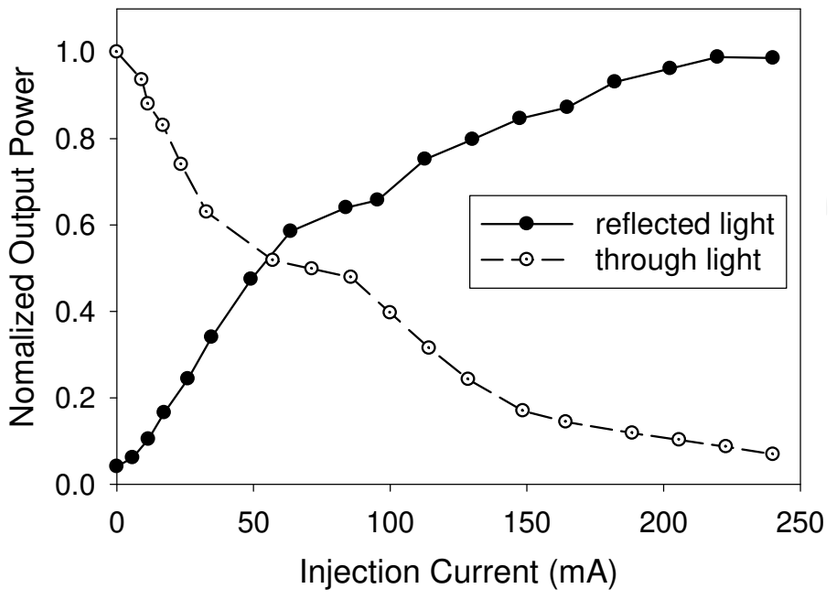

Fig. 13. Measured switching characteristics of a fabricated 2×2 double-reflection TIR optical switch.

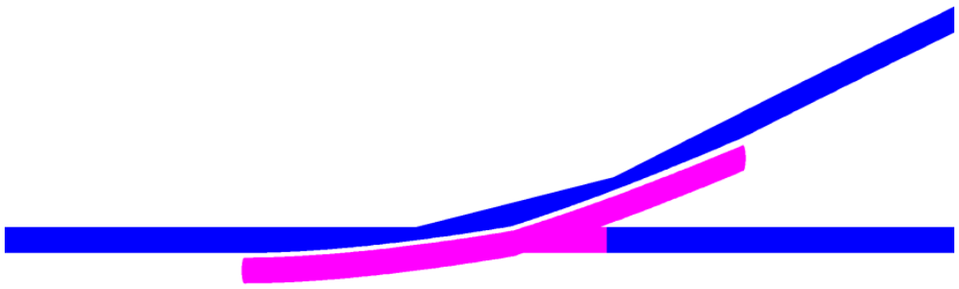

(a) Layout of the curved double-reflection electrode design

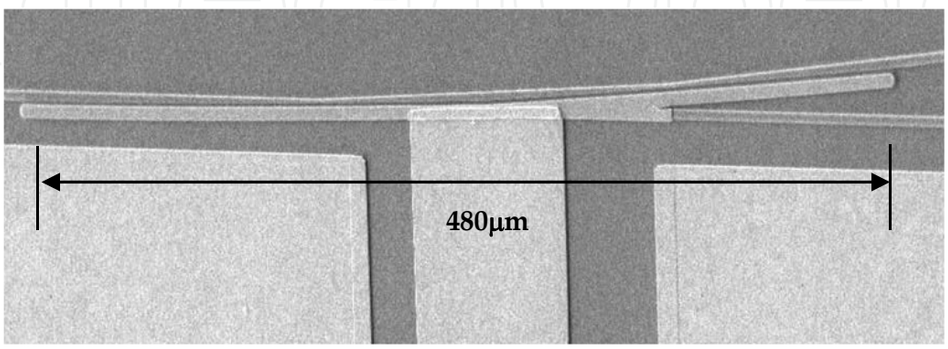

(b) SEM image of a fabricated 1×2 double-reflection TIR switch

Fig. 14. 1×2 TIR optical switch with curved double-reflection electrode.

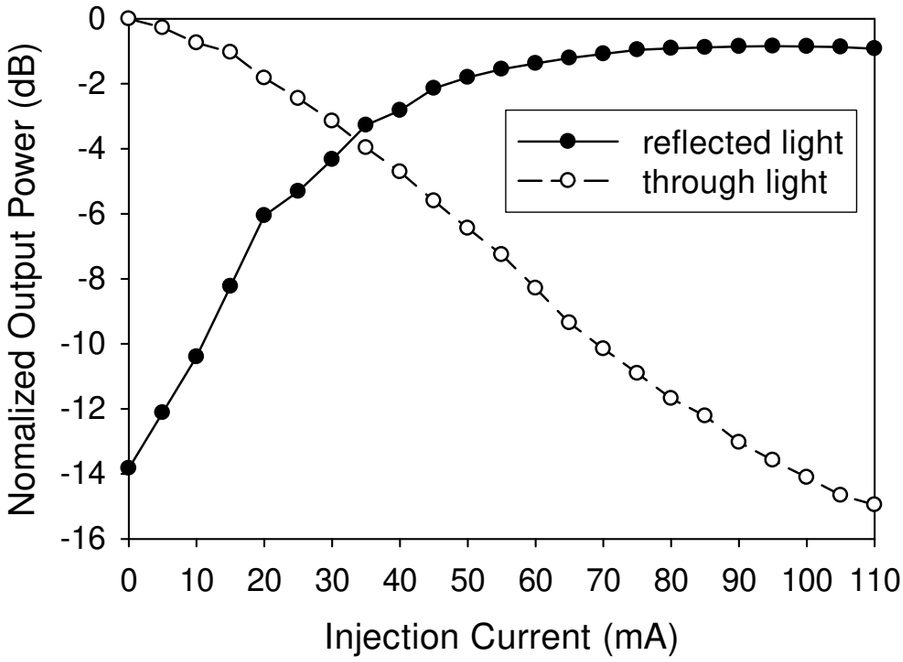

Fig. 15. Measured switching curve of a fabricated 1×2 double-reflection TIR optical switch.

3. 2×2 MMI-MZI DOS

To further reduce the switch power consumption, we have developed a 2×2 GaAs-GaAlAs carrier-injection switch based on a Mach-Zehnder Interferometer (MZI) formed by two Multi-Mode Interference (MMI) couplers. In an MZI-based switch (Cao et al., 2009; Wong et al., 2005), the two MZI arms are formed by two identical single-mode waveguides with electrodes, fabricated on the top of the waveguides, which allow the variation of the phase difference between them, based on the carrier-injection effect. Compared to the TIR switches, MZI-based switches can offer a high on-off extinction ratio and avoid the electrode fabrication complexity. More importantly, the injected current required to achieve π phase difference between the MZI arms is much smaller than that to achieve TIR, and therefore the power consumption of the MZI switches is much lower than that of the TIR devices.

A schematic of the fabricated 2×2 MMI-MZI carrier-injection switch is illustrated in Fig. 16, the device consists of an MZI configuration in which two 2×2 identical MMI couplers are connected by two identical parallel single-mode waveguides, that act as the two MZI arms. Metal electrodes are fabricated on the top of each MZI arm. Each electrode is 250 μm long and 5 μm wide. The MMI couplers are used as the 3-dB optical power splitter and combiner because of their polarization insensitive, fabrication and wavelength-tolerant properties (Besse et al., 1994). The MMI width is 20 μm and the MMI length is 1983 μm. The access (input/output) waveguides are single-mode waveguides with a width of 5 μm. Each access waveguide has two short straight sections sandwiching a long s-bend section to facilitate mode relaxation. The s-bend is designed in such a way that the additional loss caused by bending in this section is negligible.

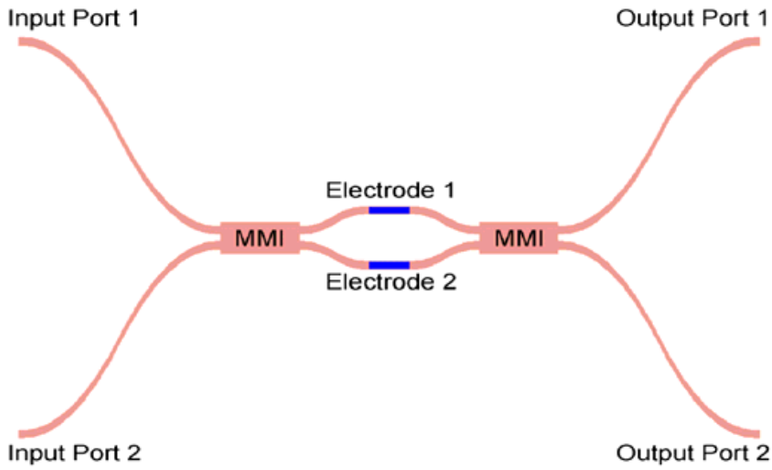

Fig. 16. Schematic diagram of a 2×2 MMI-MZI carrier-injection optical switch.

The separation between the input (output) ports is 250 μm and that between two electrodes is 35 μm. The total length of the device is about 1.4 cm. The operational principle of the 2×2 MMI-MZI switch is as follows. If two identical 2×2 MMI couplers are connected together, the two light beams, equally split from the input light by the first MMI coupler, will merge again after passing through the second MMI coupler but in the cross state. When sufficient carriers are injected into one of the electrodes to produce a π phase difference between the MZI arms, the device changes to the bar state.

The 2×2 MMI-MZI carrier-injection switch is fabricated on the epitaxial layer structure similar to the ridge waveguide structure shown in Fig. 5, with the core layer and two nearby confinement layers undoped. Compositionally graded interfaces 20 nm - 40 nm thick were used at all the layer interfaces to reduce energy band discontinuities at the heterojunctions. The calculated propagation loss of this single-mode waveguide is 0.19 dB/cm for the TE mode and 0.21 dB/cm for the TM mode.

The measured normalized output power at Output Ports 1 and 2 as a function of the injected current of Electrode 1 is shown in Fig. 17. The input light at wavelength 1.55 μm is coupled into the device at Input Port 2. As shown in Fig. 17, the first cross state (Output Ports 1 and 2 are on and off, respectively) occurs at 15.8 mA, and the first bar state (Output Ports 1 and 2 are off and on, respectively) occurs at 44.3 mA. The measured on-off extinction ratio is 20.6 dB for the cross state and 21.5 dB for the bar state. The measured voltage applied to the electrode is 1.35 V for the cross state and 1.48 V for the bar state. Therefore, the corresponding power consumption is 21.3 mW for the cross state and 65.6 mW for the bar state. Because of this very low power consumption, no extra cooling is required to maintain stable switch operation, which has been observed in our measurements. On the other hand, such low power consumption is very important for building the future optical Green Internet. From Fig. 17, we can obtain that the injected current required to achieve π phase difference between the MZI arms is 28.5 mA, which is very close to the theoretically estimated value of 29.4 mA by considering the guiding layer as an intrinsic semiconductor bulk material. Compared to the straight waveguides, the fabricated MMI-MZI devices have almost no measurable additional loss due to the MMI couplers and bend waveguides. The measured propagation loss of straight waveguides is typically around 0.5 dB/cm for a wavelength of 1.55 μm and has very small polarization dependence (< 0.5 dB). Based on

these observations, the estimated total on-chip insertion loss would be about 2 dB. The measured switching time of 15 ns is close to the carrier lifetime in the GaAs bulk material. Reducing the guiding layer thickness below 0.5 μm would increase the switching speed to a few ns but at the cost of decreasing the fibre coupling efficiency. It is noted that the switch should be at the cross state when no current is injected but this is not the case as shown in Fig. 17 due to the asymmetrical structure of the device because of fabrication errors.

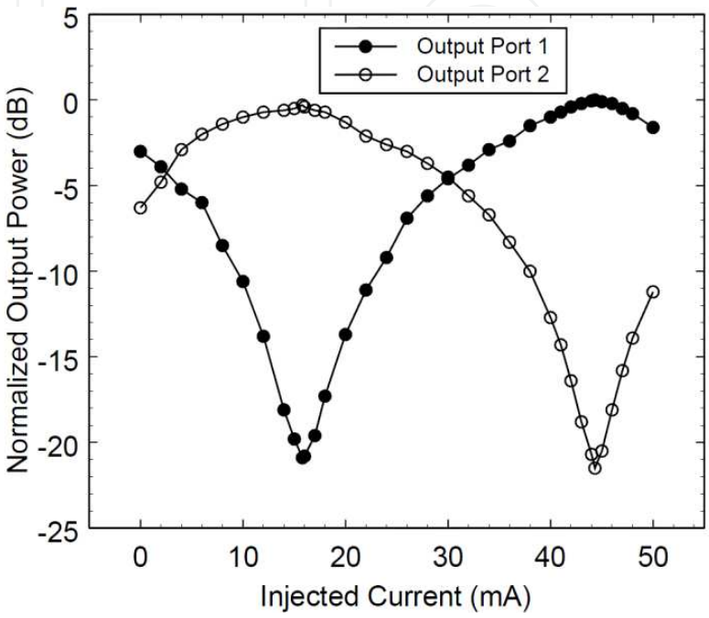

Fig. 17. Switching curves of the 2×2 MMI-MZI optical switch as a function of the injected current of Electrode 1. A light at wavelength 1.55 μm is coupled into the device at Input Port 2. The output optical power is measured at Output Ports 1 and 2.

4. Conclusions

Wide-angle 1×2 and 2×2 AlGaAs/GaAs TIR DOSs were developed by using only conventional semiconductor device fabrication technologies, suitable for monolithic circuit integration due to their small size. The developed 2×2 switch has a 7° waveguide crossing angle and a manageable maximum 0.6W dc power consumption. The 1×2 switch has a 6° branching angle and maximum quarter Watt dc power consumption. They can serve as the basic building blocks for high dense switching matrix. The techniques that we used, such as carrier restriction gap, curved electrodes, double-reflection interfaces and graded heterojunctions, can be easily applied to other switches made with other materials such as InP based, SiGe heterostructures and alike.

An ultra-low-power 2×2 MMI-MZI DOS with maximum 66 mW power consumption has also been demonstrated. Such an optical switch has a low insertion loss, high on-off extinction ratio, and very low power consumption. This device, together with the above TIR DOSs, will have significant importance in energy savings for future optical Green Internet applications, when the traffic moves down from the packet switching/routing layer to the circuit switching layer. The use of dynamic optical path-switching networks will help to accommodate users with massive video-based service demands in the future.

5. References

Abdalla, S., Ng, S., Barrios, P., Celo, D., Delage, A., El-Mougy, S., Golub, I., He, J-J, Janz, S., McKinnon, R., Poole, P., Raymond, S., Smy, T.J. & Syrett, B. (2004). Carrier Injection-Based Digital Optical Switch With Reconfigurable Output Waveguide Arms, *IEEE Photonics Technology Letters*, Vol.16, pp. 1038-1040, ISSN 1041-1135.

Agrawal, N., Weinert, C. M., Ehrke, H.J., Mekonnen, G.G., Franke, D., Bornholdt, C. & Langenhorst, R. (1995). Fast 2x2 Mach-Zehnder Optical Space Switches Using InGaAsP-InP Multiquantum-Well Structures, *IEEE Photonics Technology Letters*, Vol.7, pp. 644-645, ISSN 1041-1135.

Bennett, B. R., Soref, R.A. & Alamo, J.A.D. (1990). Carrier-Induced Change in Refractive Index of InP, GaAs, and InGaAsP, *IEEE Journal of Quantum Electronics*, Vol.26, pp. 113–122, ISSN 0018-9197.

Besse, P.A., Bachmann, M., Melchior, H., Soldano, L.B. & Smit, M.K. (1994). Optical Bandwidth and Fabrication Tolerances of Multimode Interference Couplers, *IEEE Journal of Lightwave Technology,* Vol.12, pp. 1004-1009, ISSN 0733-8724.

Cao, S., Noad, J., Sun, L., James, R., Coulas, D., Lovell, G. & Higgins, E. (2009). Small AC Driving Voltage for MZI-Based GaAs-GaAlAs Electrooptic Modulators/Switches with Coplanar Electrodes," *IEEE Photonics Technology Letters*, Vol.21, pp. 584-586, ISSN 1041-1135.

Capasso F. & Margaritondo, G. (Eds.) (1987). *Heterojunction Band Discontinuities*, Elsevier Science Ltd, ISBN 978-0444870605, Amsterdam.

Ikezawa, K., Iio, S., Suehiro, M., Suzuki, T. & Uneme, S. (2008). Demonstration of Modulation Format Free and Bit Rate Free Characteristics of 2 ns Optical Switch for Optical Routers, *Proceedings of Optical Fiber Communication Conference and Exposition*, no. JWA31, ISBN: 978-1-55752-856-8, San Diego, CA, USA, Feb 2008.

Li, B. & Chua, S.J. (2001). 2x2 Optical Waveguide Switch with Bow-Tie Electrode Based on Carrier-Injection Total Internal Reflection in SiGe Alloy, *IEEE Photonics Technology Letters*, Vol.13, pp. 206-208, ISSN 1041-1135.

Nayyer, J., Niayesh, K. & Yamada, M. (2000). Dynamic Characteristics of Optical Intersecting-Waveguide Modulators/Switches with Curved Electrodes, *IEEE Journal of Lightwave Technology,* Vol.18, pp. 693-699, ISSN 0733-8724.

Ng, S., Janz, S., Mckinnon, W.R., Barrios, P., Delage, A. & Syrett, B.A. (2007). Performance Optimization of a Reconfigurable Waveguide Digital Optical Switch on InGaAsP–InP, *IEEE Journal of Quantum Electronics*, Vol.43, pp. 1147-1157, ISSN 0018-9197.

Shimomura, K., Tanaka, N., Aizawa, T. & Arai, S. (1992). 2V Drive-Voltage Switching Operation in 1.55μm GaInAs/InP MQW Intersectional Waveguide Optical Switch, *Electronics Letters*, Vol.28, pp. 955-956, ISSN 0013-5194.

Thomson, D., Gardes, F.Y., Mashanovich, G.Z., Knights, A.P. & Reed, G.T. (2008). Using SiO_2 Carrier Confinement in Total Internal Reflection Optical Switches to Restrict Carrier Diffusion in the Guiding Layer, *IEEE Journal of Lightwave Technology,* Vol.26, pp. 1288-1294, ISSN 0733-8724.

van der Tol, J.J.G.M., Pedersen, J.W., Metaal, E.G., Ose, Y.S., Groen, F.H. & Demeester, P. (1994). Sharp Vertices in Asymmetric Y-junctions by Double Masking, *IEEE Photonics Technology Letters*, Vol.6, pp. 249-251, ISSN 1041-1135.

Wang, W.I. (1986). On the Band Offsets of AlGaAs/GaAs and Beyond, *Solid-State Electronics*, Vol.29, pp. 133–139, ISSN 0038-1101.

Wong, H. Y., Sorel, M., Bryc, A.C., Marsh, J.H. & Arnold, J.M. (2005). Monolithically Integrated InGaAs-AlGaInAs Mach-Zehnder Interferometer Optical Switch Using Quantum-Well Intermixing, *IEEE Photonics Technology Letters*, Vol.17, pp. 783-785, ISSN 1041-1135.

Yanagawa, H., Ueki, K. & Kamata, Y. (1990). Polarization- and Wavelength-Insensitive Guided-Wave Optical Switch with Semiconductor Y Junction, *IEEE Journal of Lightwave Technology*, Vol.8, pp. 1192-1197, ISSN: 0733-8724.

Zegaoui, M., Choueib, N., Harari, J., Decoster, D., Magnin, V., Wallart, X. & Chazelas, J. (2009). 2x2 InP Optical Switching Matrix Based on Carrier-Induced Effects for 1.55-μm Applications, *IEEE Photonics Technology Letters*, Vol.21, pp. 1357-1359, ISSN 1041-1135.

Zhuang, W., Duan, J., Zou, Z., Yang, P., Shi, Z., Sun, F. & Gao, J. (1996). Total Internal Reflection Optical Switch with Injection Region Isolated by Oxygen Ion Implantation," *Fiber and Integrated Optics*, Vol.15, pp. 27-36, ISSN 0146-8030.

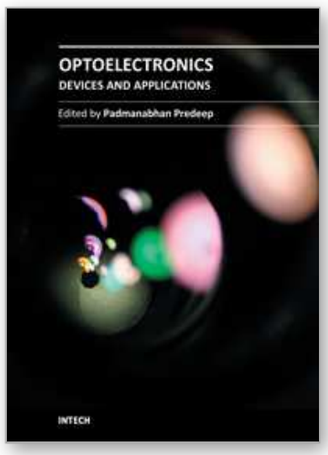

Optoelectronics - Devices and Applications

Edited by Prof. P. Predeep

ISBN 978-953-307-576-1
Hard cover, 630 pages
Publisher InTech
Published online 03, October, 2011
Published in print edition October, 2011

Optoelectronics - Devices and Applications is the second part of an edited anthology on the multifaced areas of optoelectronics by a selected group of authors including promising novices to experts in the field. Photonics and optoelectronics are making an impact multiple times as the semiconductor revolution made on the quality of our life. In telecommunication, entertainment devices, computational techniques, clean energy harvesting, medical instrumentation, materials and device characterization and scores of other areas of R&D the science of optics and electronics get coupled by fine technology advances to make incredibly large strides. The technology of light has advanced to a stage where disciplines sans boundaries are finding it indispensable. New design concepts are fast emerging and being tested and applications developed in an unimaginable pace and speed. The wide spectrum of topics related to optoelectronics and photonics presented here is sure to make this collection of essays extremely useful to students and other stake holders in the field such as researchers and device designers.

INTECH
open science | open minds

InTech Europe
University Campus STeP Ri
Slavka Krautzeka 83/A
51000 Rijeka, Croatia
Phone: +385 (51) 770 447
Fax: +385 (51) 686 166
www.intechopen.com

InTech China
Unit 405, Office Block, Hotel Equatorial Shanghai
No.65, Yan An Road (West), Shanghai, 200040, China
中国上海市延安西路65号上海国际贵都大饭店办公楼405单元
Phone: +86-21-62489820
Fax: +86-21-62489821

IntechOpen